Reprinted from

MATERIALS SCIENCE & ENGINEERING

A

Structural Materials: Properties, Microstructure and Processing

Materials Science and Engineering A268 (1999) 70–82

Spontaneous and forced shear localization in high-strain-rate deformation of tantalum

Y.-J. Chen, M.A. Meyers *, V.F. Nesterenko

Department of Applied Mechanics and Engineering Sciences, University of California, San Diego, La Jolla, CA 92093, USA

Received 16 March 1998; received in revised form 15 February 1999

ELSEVIER

MATERIALS SCIENCE AND ENGINEERING A

The journal provides an international medium for the publication of theoretical and experimental studies and reviews of the properties and behavior of a wide range of materials, related both to their structure and to their engineering application. The varied topics comprising materials science and engineering are viewed as appropriate for publication: these include, but are not limited to, the properties and structure of crystalline and non-crystalline metals and ceramics, polymers and composite materials.

Types of contributions

Original research work not already published; plenary lectures and/or individual papers given at conferences; reviews of specialized topics within the scope of the journal; engineering studies; letters to the editor.

Publication information: *Materials Science and Engineering A* (ISSN 0921–5093). For 1999, *volumes 256–272 are* scheduled for publication. Subscription prices are available upon request from the Publisher or from the Regional Sales Office nearest you or from this journal's website (http://www.elsevier.nl/locate/msea). Further information is available on this journal and other Elsevier Science products through Elsevier's website: (http://www.elsevier.nl). Subscriptions are accepted on a prepaid basis only and are entered on a calendar year basis. Issues are sent by standard mail (surface within Europe, air delivery outside Europe). Priority rates are available upon request. Claims for missing issues should be made within six months of the date of dispatch.

Orders, claims, and product enquiries: please contact the Customer Support Department at the Regional Sales Office nearest you:

New York: Elsevier Science, P.O. Box 945, New York, NY 10159-0945, USA; Tel. (+1)212-633-3730 [Toll free number for North American customers: 1-888-4ES-4ES-INFO (437-4636)]; Fax (+1)212-633-3680; E-mail usinfo-f@elsevier.com
Amsterdam: Elsevier Science, P.O. Box 211, 1000 AE Amsterdam, The Netherlands; Tel. (+31)20-4853757; Fax (+31)20-4853432; E-mail nlinfo-f@elsevier.nl
Tokyo: Elsevier Science K.K., 9-15 Higashi-Azabu 1-chome, Minato-ku, Tokyo 106-0044, Japan; Tel. (+81)3-5561-5033; Fax (+81)3-5561-5047; E-mail info@elsevier.co.jp
Singapore: Elsevier Science, No. 1 Temasek Avenue, #17-01 Millenia Tower, Singapore 039192, Tel. (+65)434-3727; Fax (+65)337-2230; E-mail asiainfo@elsevier.com.sg
Rio de Janeiro: Elsevier Science, Rua Sete de Setembro 111/16 Andar, 20050-002 Centro, Rio de Janeiro - RJ, Brazil; Tel. (+55)21-5095-340; Fax (+55)21-507-1991; E-mail elsevier@campus.com.br [Note (Latin america): for orders, claims and help desk information, please contact the Regional Sales Office in New York as listed above]

Abstracting and/or Indexing Services

American Ceramic Society; Cambridge Scientific Abstracts; Chemical Abstracts; Current Contents; Engineering Index; FIZ Karlsruhe; Fluid Abstracts; Fluidex; Glass Technology Abstracts; Inspec/Physics Abstracts; Metals Abstracts; Pascal (Centre National de la Recherche Scientifique); Physikalische Berichte; Research Alert™; Science Citation Index.

ELSEVIER

Materials Science and Engineering A268 (1999) 70–82

MATERIALS SCIENCE & ENGINEERING A

Spontaneous and forced shear localization in high-strain-rate deformation of tantalum

Y.-J. Chen, M.A. Meyers *, V.F. Nesterenko

Department of Applied Mechanics and Engineering Sciences, University of California, San Diego, La Jolla, CA 92093, USA

Received 16 March 1998; received in revised form 15 February 1999

Abstract

High-strain-rate shear localization was induced in tantalum by (a) lowering the deformation temperature or (b) subjecting it to high strains by dynamic deformation (up to $\varepsilon_t = -0.8$) or (c) pre-shocking (at $\varepsilon_{eff} = 0.22$) and then deforming it. Although at ambient temperature the deformation of tantalum is macroscopically uniform to high strains ($\varepsilon_t \cong -0.8$), at 77 K shear localization under the same loading condition was developed at a critical strain of -0.2 to -0.3. This higher propensity to shear localization at low temperatures is a direct consequence of the combination of lower heat capacity and higher rate of thermal softening. At the three temperatures investigated (77, 190 and 298 K), localization occurs at strains significantly higher than the instability strains (the maxima of the adiabatic stress–strain curves for these three temperatures). The thicknesses of the forced localization regions and shear bands were found to be a function of temperature, and decreased with decreasing temperature (at the same strain) in accord with the equation proposed by Y. Bai et al. (Y. Bai, C. Cheng, S. Yu, Acta Mechanica Sinica 2 (1986) 1). Shock deformation of tantalum enhances its predisposition to subsequent shear localization, and this was demonstrated by subjecting shocked and unshocked specimens to high strain, high strain rate deformation through the collapse of a thick-walled cylinder assembly.

Keywords: Tantalum; Shear localization; High-strain-rate deformation

1. Introduction

The two outstanding physical properties of tantalum (high density and ductility) have made it into a very attractive material for ballistic penetration devices, such as shaped charges and explosively-forged projectiles [1]. A considerable number of investigations have been conducted over the past 10 years, which emphasize the ductility and homogeneous deformation characteristics of this metal [2–9] in contrast with tungsten, that undergoes a ductile-to-brittle transition as the strain rate is increased [10]. There is only limited information, by Worswick et al. [3], and Qiang et al. [4] of shear localization in a tantalum explosively-forged projectile; the present authors and LaSalvia et al. [11–14] also observed shear localization in thick-walled cylinders that had been collapsed through explosives.

The primary objective of the investigation whose results are reported herein was to quantitatively establish, (1) the conditions for shear localization and (2) material behavior under forced localized shear. In order to promote localization, the initial temperature was decreased and material mesostructure was pre-conditioned by shock compression. Earlier experiments by Andrade et al. [15] and Meyers et al. [16] on copper had revealed that shock conditioning decreased the thickness of the forced localized shear regions and enhanced the intensity of the plastic deformation produced using hat-shaped specimens under the same deformation conditions. The term 'forced localized shear' is used here to emphasize the fact that in hat-shaped specimens the origin of localization is rooted in the initial conditions of loading and geometry of the specimen. This localized shear is not created by instability in uniformly strained material and will be observed in any material using hat-shaped specimens. Both the decrease in deformation temperature and shock conditioning increase the

* Corresponding author. Tel.: +1-619-534-4719.
E-mail address: mameyers@ames.ucsd.edu (M.A. Meyers)

0921-5093/99/$ - see front matter
PII: S0921-5093(99)00110-0

flow stress and hence the heat generated per unit of strain in subsequent plastic deformation; the thermal softening is also different. Thermal softening is higher at lower temperatures because of the shape of activation barriers opposing dislocation motion, and Andrade et al. [15] showed, for copper, that it is altered by shock conditioning, with a rapid drop at the recrystallization temperature.

2. Material and experimental techniques

The tantalum used in the present investigation has characteristics, processing, and texture described by Meyers et al. [5]. The tantalum plate was produced and processed by Cabot. The plate (8 mm thick) was produced by press forging 30-cm high ingots into 10-cm slabs, which were annealed. This was followed by cross-rolling to the final thickness with intermediate anneals. No final anneal was performed. The final material shows a considerable texture, that is given by Meyers et al. [5]. Its average grain size is 41 μm and it has the following impurities (ppm), C: 60; N: 10; O: 70; H: 4. The dislocation density was equal to 10^9 cm^{-2}; this is due to the fact that deformation was applied after the last annealing step and the structure is lightly work hardened.

Shock compression was applied using an explosively accelerated flyer plate in a parallel, normal impact geometry. Details of the experimental set-up are described by Murr et al. [9]. The shock amplitude was 45 GPa, with a corresponding pulse duration of 1.8 μs and at an initial temperature of 300 K. Pre-shocking generated a considerable density of deformation twins (in addition to a high dislocation density), which resulted in a hardening of the material that exceeded the hardening obtained under quasi-static uniaxial compression to the effective strain equal to the transient strain (0.22) imparted by shock compression [9].

Three complementary testing methods were used to initiate shear localization and forced localized shear in tantalum: (1) uniaxial compression tests; (2) hat-shaped specimen tests; and (3) the thick-walled cylinder tests. Uniaxial compression tests performed in a Hopkinson–Kolsky bar lead to the spontaneous formation of shear bands under the appropriate conditions. The same occurs with the thick-walled cylinder test, in which a gradient of plastic strain is established during the collapse; it is possible to evaluate the initiation strain as well as the propagation trajectory. In the hat-shaped technique, on the other hand, the localization is forced by the geometry of the specimen, and the shear localization is not initiated by instability but by the external tractions and sharp corners. These three techniques are briefly described below.

2.1. Uniaxial compression tests

Uniaxial quasi-static and dynamic tests were carried out in a SATEC testing machine and split Hopkinson–Kolsky bar, respectively. The specimens were spark-eroded and had a cylindrical shape. They had a diameter of 5 mm and different lengths: 4, 5, and 7.5 mm. When true compressive strains in the range of $0.8 \sim 1.0$ are required, a longer gage length was used to ensure a reasonable degree of uniaxiality and uniformity in the stresses. The split Hopkinson–Kolsky bar was used with 12.7-mm diameter bars and data were collected using a data acquisition board (with 10 megasamples per s) in an IBM compatible computer. The high-strain-rate tests were carried out at two nominal strain rates: 3.5×10^3 and 5.5×10^3 s^{-1}. Experiments were carried out at 77, 190 and 298 K. The low-temperature experiments were conducted using liquid nitrogen (77 K) and a liquid nitrogen–methanol mixture (190 K). It was pointed out that frictional effects can be higher at low temperatures because of the freezing of the lubricant. This could have been an additional contributory factor for shear localization.

2.2. Hat-shaped specimen tests

The hat-shaped specimen was developed by Meyer and Manwaring [17] and has been successfully used in the study of high-strain, high-strain-rate deformation of metals in conditions of forced localized shear. Although initially designed for steels, it has also been applied to copper [15,16], titanium [18], aluminum alloys [19], and tantalum [5]. For this research, a smaller geometry was used due to the limited availability of material. The specimen dimensions are shown in Fig. 1(a). The bars compress the specimen and force the shear deformation into a narrow region shown in Fig. 1(b,c). The total displacement is established by a spacer ring, that limits the relative motion of the two parts of the 'hat'. The diameter of the top part is slightly larger (7.6 mm) than the internal hole diameter (7.5 mm) in order to superimpose a small compressive stress laterally on the shear region.

2.3. Thick-walled cylinder tests

The thick-walled cylinder technique was developed by Nesterenko and Bondar [20] and is described, for the specific configuration used here, by Nesterenko et al. [12] and Chen et al. [14]. In contrast with the hat-shaped specimen technique, in the thick-walled cylinder technique shear localization starts from macroscopically uniformly deformed samples in a state of pure shear. Both as-received and shock-compressed tantalum were tested in this configuration, in order to establish the effect of shock loading on the propensity for shear localization.

3. Results and discussion

3.1. Compression tests

The susceptibility to shear band formation, or critical strain at the onset of shear localization, has been analytically expressed by a number of researchers, starting with Recht [21]. Bai and Dodd [22] provide a systematic comparison. Clifton [23] considered the key elements for establishing the strain for shear localization:

$$\left[\frac{1}{\tau}\left(\frac{\partial\tau}{\partial\gamma}\right)+\frac{\beta}{\rho C_v}\left(\frac{\partial\tau}{\partial T}\right)\right]m\dot{\gamma}+\frac{\lambda\xi^2}{\rho C_v}>0 \quad (1)$$

where τ is the stress, γ is the strain, ρ is the density, C_v is the heat capacity, β the fraction of work converted into thermal energy, λ is the thermal conductivity, and

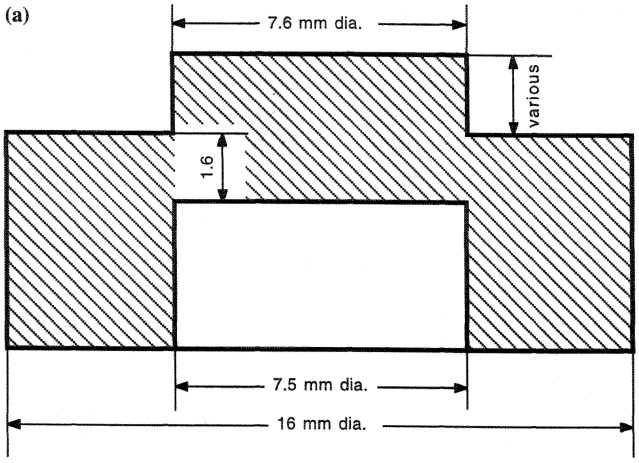

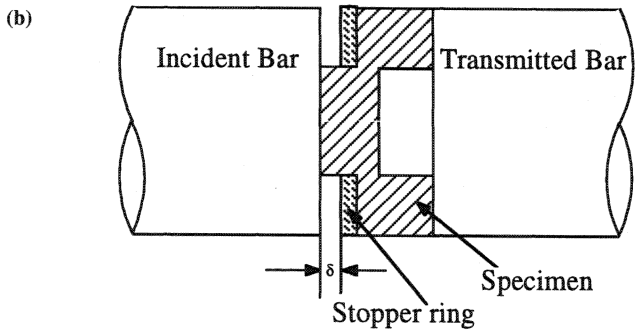

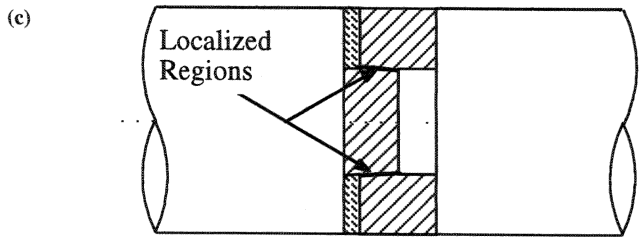

Fig. 1. (a) Dimensions of hat-shaped specimen, and its loading configuration in split Hopkinson–Kolsky bar (b) before and (c) after impact.

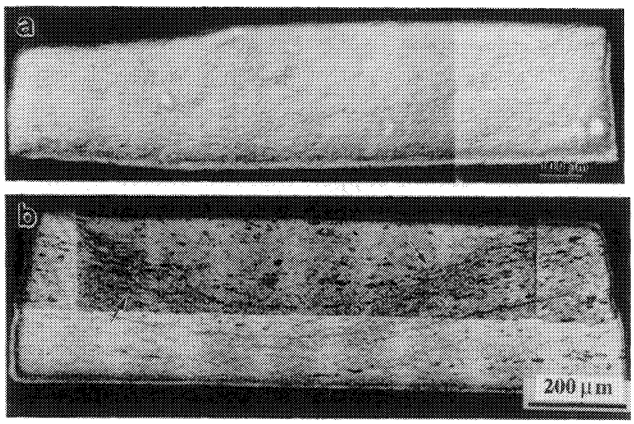

Fig. 2. Cross-section of the cylindrical compression specimens at room temperature and $3.5 \times 10^3\ s^{-1}$; (a) as-received, deformed to a plastic strain of -0.7, showing no shear bands, (b) shocked, deformed to strain of -0.65, showing diffuse shear bands (marked by arrows).

ξ is a constant that quantifies the initial perturbation (it is the reciprocal of the wavelength of the initial inhomogeneity). It is well-known that high τ, $\frac{\partial\tau}{\partial T}$, and low C_v, $\frac{\partial\tau}{\partial\dot{\gamma}}$, m (strain rate sensitivity) favor localization. The role of thermal conductivity and the perturbations is also included in Clifton's analysis. The magnitude of perturbations has a direct bearing on the localization strain. This approach does not incorporate directly metallurgical properties, such as grain size and crystallographic changes, during deformation.

No shear localization could be macroscopically observed in as-received tantalum at strain rates up to 7000 s^{-1} at ambient temperature in the cylindrical compression specimens with nominal dimensions of $\phi 5 \times 4$ mm. This is in agreement with earlier results by Meyers et al. [4] and Gray et al. [6]. Fig. 2(a) shows the cross-section of an as-received tantalum specimen deformed to a compressive true plastic strain of -0.7 at ambient temperature and at $3.5 \times 10^3\ s^{-1}$. There is no sign of shear localization in the entire cross-section. Shear bands were also absent up to a true strain of -1.0 at ambient temperature at this strain rate. However, Fig. 2(b) shows the existence of shear bands in the pre-shocked tantalum specimen (see arrow), deformed to -0.65 at the same strain rate and temperature. This is attributed to the higher flow stress imparted by shock loading. The shear bands in Fig. 2(b) are not fully developed and are rather diffuse. This is connected with the well-known dependence of shear localization on thermal properties and flow stress. Fig. 2 illustrates the significance of higher flow stress in shear band formation since shock loading does not alter the thermal properties; shock loading increases the flow stress from 700 to 900 MPa and this represents a $\sim 29\%$ increase in thermal energy production per unit strain.

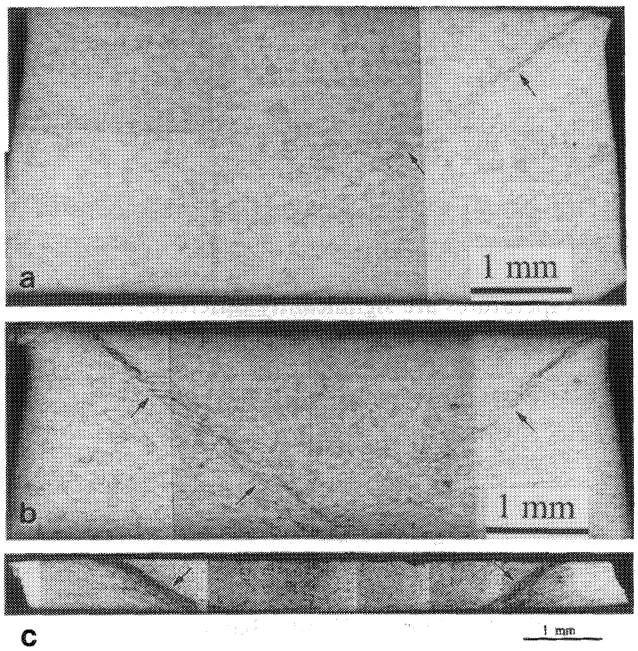

Fig. 3. Shear band formation at 77 K and 5500 s^{-1} in continuous (adiabatic) deformation, (a) $\varepsilon_t = -0.23$, (b) $\varepsilon_t = -0.3$, and (c) $\varepsilon_t = -0.65$.

It is well known that lowering the deformation temperature also results in an increase in flow stress. It can then be easily seen that the propensity to shear localization is higher at low temperatures. Indeed, Chin et al. [24] demonstrated that even aluminum formed shear bands when deformed quasistatically at 4.2 K. At room temperature, aluminum is one of the most ductile materials. The development of shear localization in continuous (adiabatic) deformation of tantalum at 77 K is shown in Fig. 3. The following features can be seen: (a) initiation of shear localization, (b) and (c) growth of shear bands with increasing strain. Fig. 4 shows multiple shear bands in a specimen that was triple-loaded with a total strain of -0.6 at 77 K and 5500 s^{-1}. The incremental strains were -0.14, -0.18, and -0.28. The shear bands in Fig. 4 basically belong to two systems and their formation is believed to occur in the second and third increments of deformation experienced by the specimen. Although the specimens in Fig. 3 were tested at the same temperature and strain rate as

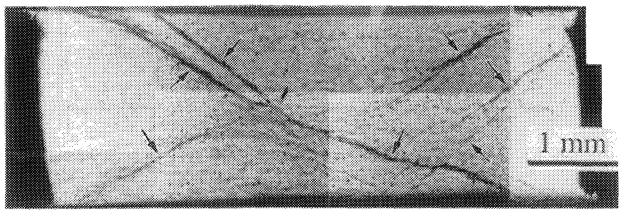

Fig. 4. Shear band formation in incremental tests at 77 K and 5500 s^{-1} with total strain of -0.6 (strains for increments were -0.14, -0.18, and -0.28).

that in Fig. 4, the band structure is somehow more diffuse than in Fig. 4 (the thicknesses of shear bands in Figs. 3 and 4 are ~ 200 and ~ 50 μm, respectively).

The decrease of heat capacity at low temperatures also plays a significant role in shear localization. The heat capacity decreases at temperatures below 300 K while the thermal conductivity varies only slightly. At low temperatures, due to lower heat capacity, the same amount of plastic work will result in a higher temperature rise. This enhances the susceptibility to the formation of shear localization. An enhanced thermal diffusivity would tend to increase the thickness of the shear band, resulting in a diffuse shear band; however this is not the case because it only increases significantly below 77 K.

In order to better understand the deformation behavior, a constitutive description is needed; the Zerilli–Armstrong model is used here. Zerilli and Armstrong [25] developed a constitutive equation for BCC metals and applied it to tantalum, based on the results by Bechtold [26], Hoge and Mukherjee [27], and Mitchell and Spitzig [28]. The constitutive equation is given below:

$$\sigma = \sigma_G + B_0 e^{-(\beta_0 - \beta_1 \ln \dot{\varepsilon})T} + K\varepsilon^n + kd^{-\frac{1}{2}} \quad (2)$$

σ_G is the athermal portion of the stress, n the work hardening exponent, d the grain size, and β_0, β_1, B_0, K, and k are parameters. Because of the different chemistry and processing history of the material used in this research, a new set of parameters for this model had to be determined from experiments. The thermal and strain rate responses were experimentally determined and are given in Fig. 5, along with the data of Hoge and Mukherjee [27]. To minimize the deviation at high strain rates, the strain hardening parameters were determined with the test results at a strain rate of 3500 s^{-1} and room temperature (Fig. 6a). These are interrupted tests described by Meyers et al. [4], which provide a quasi-isothermal curve, from which the adiabatic curve can be obtained. In the interrupted tests, the specimen is allowed to return to the initial temperature after each increment of strain. Several (three or more) sequential deformation cycles are applied to the specimen, and the envelope of the stress–strain curves provides a good approximation of the isothermal curve. These interrupted experiments were introduced by Wittman et al. [29]. The parameters of the Zerilli–Armstrong model are given in Table 1 and compared to those obtained by Zerilli and Armstrong [25] for Hoge and Mukherjee's data. The continuous lines in Fig. 5(a,b) represent the application of the Zerilli–Armstrong equation to the various temperatures and strain rates of interest. Fig. 6(a) shows the test curves and the predictions of Zerilli–Armstrong model under both isothermal and adiabatic conditions at 298 K and 3500 s^{-1}, and Fig. 6(b)

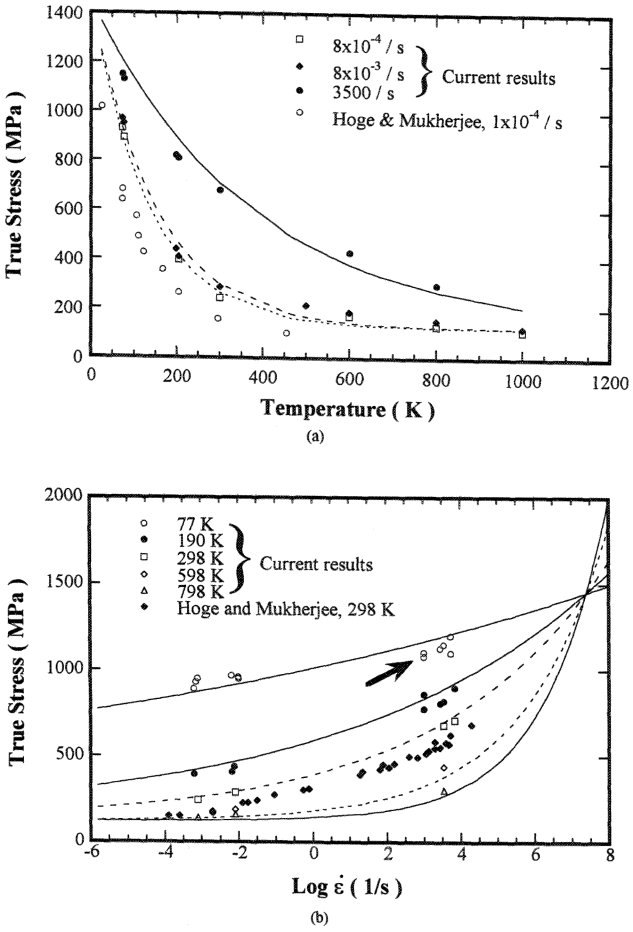

Fig. 5. (a) Temperature and (b) strain rate dependence of flow stress of tantalum.

shows the equivalent curves for 190 K and 5500 s^{-1}. The upturn of the measured curves in Fig. 6(b) was due to the contact of stopper ring by the incident bar during the tests. The stopper ring was used to limit the deformation to a prescribed value, whereas for the 298 K curves a special Hopkinson–Kolsky bar wave trapping device was used [5].

Also shown in Fig. 6(a) is the prediction of adiabatic temperature from the Zerilli–Armstrong model at 298 K and 3500 s^{-1}. The adiabatic temperature of the plastically deformed specimen was estimated by assuming the conversion of 90% plastic work into heat. Due to the form of the Zerilli–Armstrong equation, the adiabatic temperature as a function of strain has to be obtained with a numerical method.

At low temperatures and high strain rates, the prediction of yield stress by Zerilli–Armstrong model is higher than the experimental results in Fig. 5; this is indicated by an arrow. This is attributed to the change of the predominant deformation mechanism from dislocation slip to twinning at low temperatures and high strain rates. Therefore, great attention was paid to the experimental data at low strain rates; high-strain-rate data for room temperature and above only were used for constructing the model. Mechanical twinning in high strain rate testing at both 77 and 190 K was observed in every test. The current constitutive models do not take the slip-twinning transition into effect, and Zerilli and Armstrong [30] have recently discussed the importance of including twinning into the constitutive response. Fig. 7 shows the mechanical twins formed at 190 K and 5500 s^{-1}. The mechanical twins formed at low temperatures are significantly different from shock-induced twins reported by Murr et al. [9] in the same tantalum. The low temperature twins are usually larger in size and have a lower frequency of occurrence. In shock compression, the high stress (45 GPa) provides a large driving force for mechanical twinning which results in a high nucleation rate. The size of twins was limited by the large number of twins themselves (twin–twin intersections) and by the limited time of pulse duration (1.8 μs); in contrast, the duration of the stress pulse in the Hopkinson–Kolsky bar is ~100 μs.

The critical strains for shear localization at 77 and 190 K were determined in uniaxial compression at two levels of strain rate: 3500 and 5500 s^{-1}. The critical

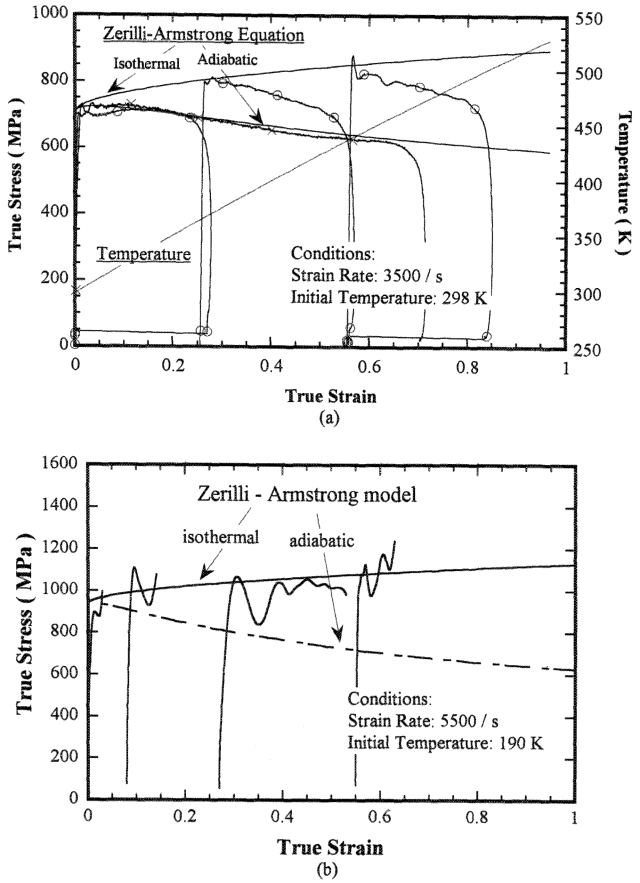

Fig. 6. Interrupted (quasi-isothermal) and continuous (adiabatic) tests and the prediction of Zerilli–Armstrong model, (a) quasi-isothermal and adiabatic tests at 298 K and 3500 s^{-1}; (b) quasi-isothermal test at 190 K and 5500 s^{-1}.

Table 1
Parameters of Zerilli–Armstrong equation for tantalum

	$\sigma_G + kd^{-\frac{1}{2}}$	B_0	β_0	β_1	K	n
Current	122	1330	0.00525	0.000308	197	0.5
Hoge–Mukherjee	30	1125	0.00535	0.00327	310	0.44

strains were -0.34 and -0.23 at 77 K, and -0.65 and -0.5 at 190 K, respectively. The results are plotted in Fig. 8 along with the computed instability strain using the Zerilli–Armstrong model with the parameters given in Table 1. The instability strain is taken as the maximum in the adiabatic stress–strain curve and is mathematically expressed by:

$$\frac{d\sigma}{d\varepsilon} = -B(\beta_0 - \beta_1 \ln \dot{\varepsilon})\frac{dT}{d\varepsilon}e^{-(\beta_0 - \beta_1 \ln \dot{\varepsilon})T} + Kn\varepsilon^{n-1} = 0 \quad (3)$$

The equation has to be solved numerically. The instability strain increases with temperature; this is the direct result of the interplay among the various parameters. In this particular case, both the higher thermal softening rate ($d\sigma/dT$) and lower heat capacity, contribute significantly to a lower instability strain.

Wright and Walter [31] discuss at length the two separate phenomena of instability and localization, and note that the former is a necessary condition for the latter. Consistent with their prediction, the localization strains (experimentally obtained), are substantially higher than the instability strains. They are also shown in Fig. 8. It is interesting to note that both the instability and localization strains increase with temperature. It can also be seen that the temperature dependence of critical strain for localization and instability are significantly different. The large gap in Fig. 8 between the critical strains for shear localization and the corresponding instability strains is consistent with the theoretical predictions on the separation of instability and shear localization [32–37]. At ambient temperature, instability occurs at the strain of -0.1 at a strain rate of 3500 s^{-1}, as shown in Fig. 8, while the shear localization was not observed at a strain of -0.7 and required a long specimen to manifest itself. At 77 K, instability occurred almost at the beginning of deformation, while localization did not appear until the strain accumulated to -0.34. It should be mentioned that the development of instability is a function of strain rate, and was modeled by Wright and Walter [31]. The instability strain, where the maximum stress is observed, decreases with increasing strain rate or decreasing temperature, as shown in Fig. 9.

The importance of thermal properties in shear localization is revealed in the works on low temperature instabilities, that can be traced back to the 1950s when Basinski [38] first proposed the existence of thermo-mechanical instability at low temperatures due to the decrease of the heat capacity. This type of instability is also called adiabatic instability. Usually, adiabatic instability occurs in tensile testing, although it was also reported in compression test for tantalum single crystals at liquid helium temperature [39]. Since the heat capacity of a material is reduced as the temperature is lowered, the adiabatic temperature rise per increment of plastic work will be greater. Hence, materials have a higher propensity to shear localization in low temperature deformation.

The absence of shear localization at ambient temperature can be clearly seen in Fig. 2(a), despite the

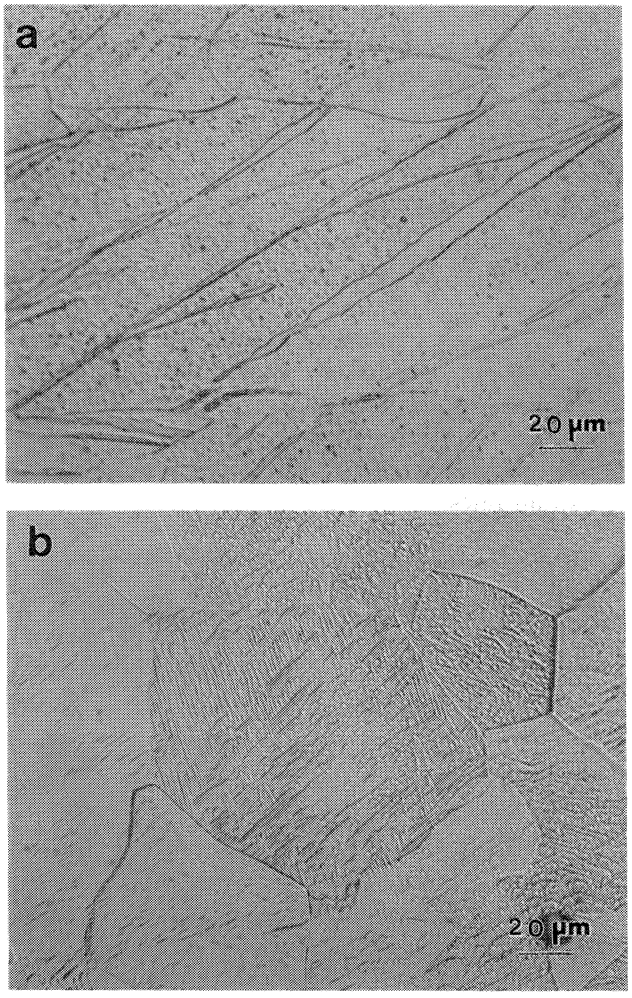

Fig. 7. Mechanical twinning formed (a) by deformation at 190 K and 5500 s^{-1}, and (b) by shock compression to a pressure of 45 GPa.

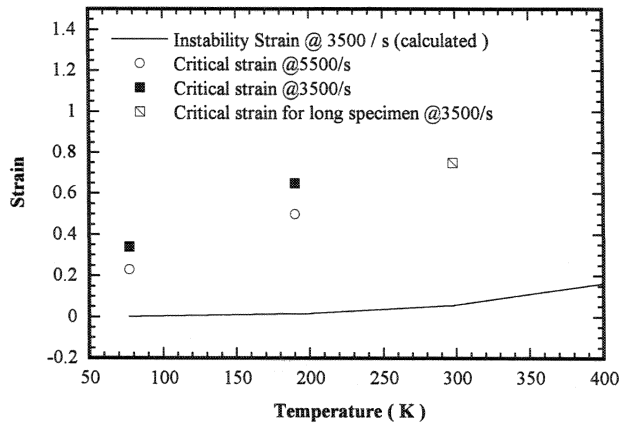

Fig. 8. Critical strains for shear localization in different deformation conditions, and computed instability strain as a function of temperature, using Zerilli–Armstrong model with parameters given in Table 1.

corresponding adiabatic stress–strain curves in Figs. 6 and 9 showing the occurrence of instability (i.e. a negative slope in the curve). This phenomenon is consistent with earlier results by Meyers et al. [18] for titanium. They observed that the occurrence of unstable plastic flow preceded shear localization by a significant amount of strain. Meyers et al. [18] also provided a microstructural interpretation in terms of dynamic recrystallization. They suggested that instability in titanium is produced by the increase of temperature, enhancing the mobility of dislocations, while localization requires dynamic recovery/recrystallization.

Increasing the strain rate has the same effect on the onset of shear localization as decreasing the temperature. This is similar to the relationship of the effects of strain rate and temperature on flow stress. However, the influence of strain rate on the initiation of shear localization is a more complicated issue than that of temperature, and inertial effects come into play at very high strain rates.

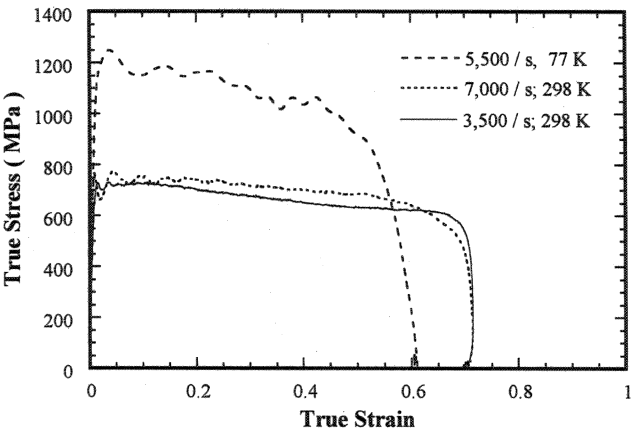

Fig. 9. Adiabatic stress–strain curves at different strain rates and temperatures; note the change of instability strains.

Table 2 lists the effects of specimen dimension and deformation conditions on the formation of shear localization. When localization occurs after significant plastic strain, frictional end effects play an important role and can delay the phenomenon. The uniaxial stress state can be retained to larger plastic strains if the length/diameter ratio is increased. In Table 2, the longer specimens show a higher propensity to shear localization. Fig. 10 shows the microstructure of this long specimen at room temperature and 3500 s^{-1}. The shear localization observed at room temperature is more diffuse than at 77 K. These results confirm that lowering the deformation temperature enhances the localization.

3.2. Hat-shaped tests

The objective of the experiments with the hat-shaped specimens was to probe the development of forced shear localization, and to compare their thickness with shear band thickness. The initiation of localized shear is due to the particular geometry of hat-shaped specimens. The specimens were subjected to different displacements at a nominal local strain rate of 4×10^4 s^{-1} (inside the localized shear regions). As-received tantalum was tested at temperatures of 77, 190 and 298 K, while shocked tantalum was tested at 298 K only.

Fig. 11 shows the microstructures of the localized shear regions deformed at 77, 190 and 298 K with different displacements. The shear strains were estimated by dividing the displacement by an approximate shear localization thickness, L, as indicated in Fig. 11(d). This method is not very rigorous, since the thickness of the shear band is not constant and the shear strain varies with distance from the central area. Additionally, the shear strain near both ends of the localized shear regions is the highest. Table 3 lists the measured thicknesses and shear strains of the localized shear regions at different initial temperatures and for different displacements, and the maximum calculated temperatures inside localized shear regions. The maximum temperature increases with shear strain.

It is clear from Fig. 11 that the development of localized shear regions occurred progressively with increasing of shear strain. While a clear localized shear region is seen at a displacement of 0.3 mm ($\gamma = 3.0$) and 77 K, at room temperature higher strains are needed; the localization only manifested itself for a displacement of 0.5 mm ($\gamma = 2.5$). The development of the localized shear regions can also be seen with decreasing initial temperatures. The thicknesses of these regions are ~ 200 μm at 298 K, ~ 190 μm at 190 K, ~ 80 μm and ~ 130 μm at 77 K. Fig. 11 shows the thickness of the localized shear region increasing with shear strain at 77 K.

Table 2
Dimensional effect on the formation of shear localization

Sample dimensions (mm)	Temperature (K)	Strain rate (s^{-1})	True strain	Localization
$\phi 5 \times 4$	298	3500	1.0	No
$\phi 5 \times 7.5$	298	3500	0.7	Yes
$\phi 5 \times 8$	298	6×10^{-4}	0.5	No
$\phi 5 \times 4$	77	5500	0.23	Yes
$\phi 10 \times 8$	77	5500	0.3	No

Fig. 12 shows the development of shear localization region at room temperature for shocked tantalum. The thickness increases from 130 to 180 μm when displacement increases from 0.5 to 1.4 mm. Because shocked tantalum has a higher flow stress than as-received, a narrower and sharper localized shear region was produced with the same displacements as their as-received counterparts (compare with Fig. 11).

Shear stress-displacement curves can be obtained during the deformation of a hat-shaped specimen. This is a considerable advantage of this experimental method over the thick-walled cylinder method. Fig. 13 shows the shear stress-displacement curves at all three temperatures. The curves show a plateau at different shear stress levels for different initial temperatures and a sharp increase in shear stress when the stopper ring is contacted. Fig. 13 also illustrates the increasing shear stress with the decrease of the initial temperature. In conjunction with the measurement of the localized shear thickness listed in Table 3 and the microstructures in Fig. 11, it can be stated that the higher shear stress produces thinner localized shear and requires smaller displacement to generate fully-developed localized shear regions. These experimental results confirm that the thickness of a localized shear is directly proportional to the adiabatic temperature inside the region and inversely proportional to the shear stress.

It is well known that two counterbalancing factors strongly influence the growth of localized shear regions: heat generation due to plastic work and heat dissipation via heat conduction. In the hat-shaped specimens the forced localization regions are governed by the same effects. It is therefore reasonable to extend the analyses on the shear band growth to the study of the growth of the localized shear region in hat-shaped specimens. The thickness of shear bands has been satisfactorily predicted analytically and numerically with perturbation analyses [22]. The contribution of heat conduction to the thickness of a shear band was included in these analyses [40–42]. The simplest among all predictions is due to Bai et al. [40,41] who have proposed the following equation for the thickness, L of a shear band:

$$L = 2\sqrt{\frac{\lambda T_{max}}{\beta \tau \dot{\gamma}}} \quad (4)$$

where λ is thermal conductivity, T_{max} is the maximum temperature inside the shear band, τ is the shear stress acting in the shear bands, and $\dot{\gamma}$ is the strain rate. β is the fraction of plastic work converted to thermal energy, which is usually taken as 0.9. In Eq. (4), thermal conductivity and maximum temperature inside the shear band have a positive effect on the thickness of shear bands, while strain rate and stress have a negative effect. This relationship is generally consistent with other more complicated models which predict shear band thickness [22]. For tantalum, thermal conductivity is fairly constant at temperatures above 77 K. At a fixed strain rate, such as 4×10^4 s^{-1}, typical for the hat-shaped specimens in the current research, from Eq. (4), the thickness of shear bands can be considered as a linear function of $\sqrt{T_{max}/\tau}$, the square root of the ratio of maximum temperature, T_{max} inside the shear band and the applied shear stress, τ, on the shear band.

Although the localized shear regions in hat-shaped specimens were forcedly initiated upon deformation with an especially designed geometrical imperfection, they were still developed into different thicknesses at different deformation conditions. Table 3 provides the experimental parameters. The maximum adiabatic temperatures were calculated using Zerilli–Armstrong constitutive models. Since all the hat-shaped specimens were tested at the same strain rate (4×10^4 s^{-1}), the aforementioned linear analysis can be readily applied. The applied shear stresses were determined from Fig. 13. The minimum shear stress in each test was taken as the shear stress corresponding to the thermo-mechanical conditions experienced by the particular sample at the end of its deformation, because the strain was obtained at the end of deformation.

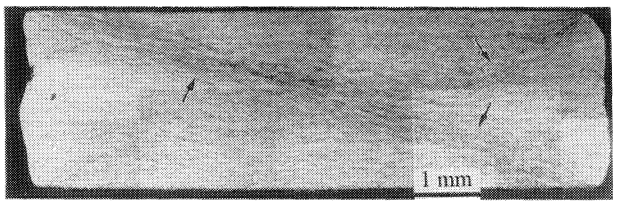

Fig. 10. Cross-section of 7.5-mm specimen deformed at room temperature and 3500 s^{-1} to a strain of -0.8; shear bands marked by arrows.

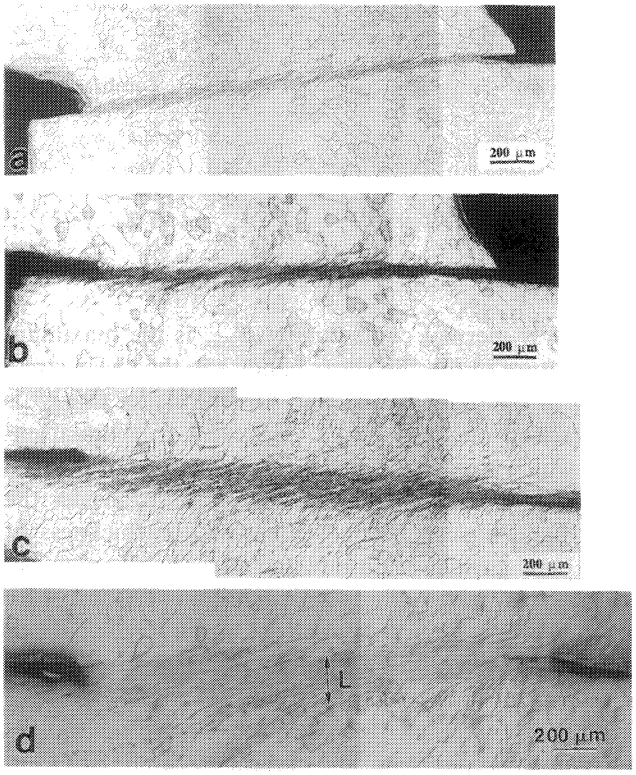

Fig. 11. Hat-shaped specimens of as-received tantalum deformed at different temperatures and displacements: (a) 0.3 mm at 77 K; (b) 0.5 mm at 77 K, (c) 1.0 mm at 190 K, and (d) 1.4 mm at 298 K.

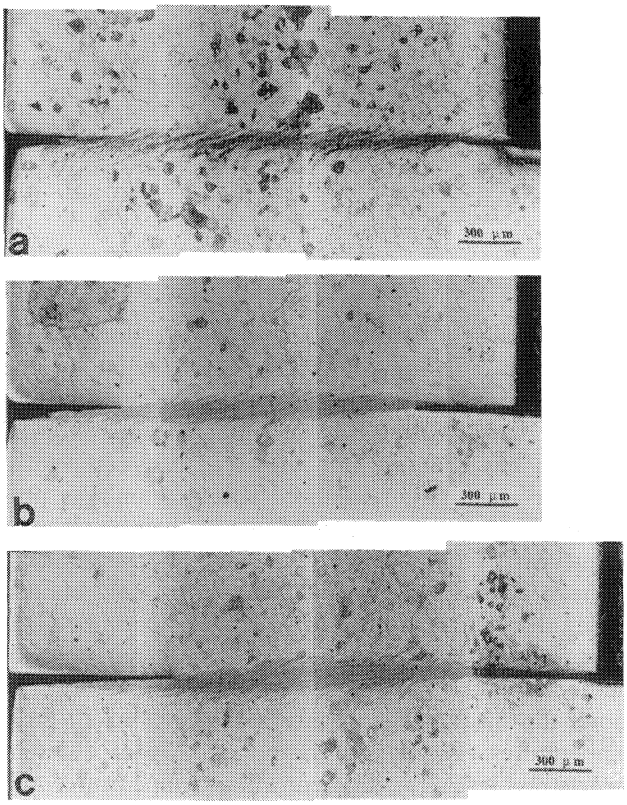

Fig. 12. Hat-shaped specimens of shocked tantalum deformed at 298 K and different displacements: (a) 0.5 mm, (b) 1.0 mm and (c) 1.4 mm.

Fig. 14 shows the thickness of the localized shear regions; L is plotted against $\sqrt{T_{max}/\tau}$. Linear regression analysis was applied to the data of the localized shear regions. The correlation coefficient, R is equal to 0.951, showing the existence of a good linear relationship between L and $\sqrt{T_{max}/\tau}$. The linear regression slope is 0.114.

Also plotted in Fig. 14 is the thickness predicted using Eq. (4). The slope of 0.080 was calculated from $2\sqrt{\lambda/\beta\dot{\gamma}}$, where $\lambda = 59$ W/m^2 K, $\dot{\gamma} = 4 \times 10^4$ s^{-1} and β is the conversion of plastic work to heat (90%). The predicted slope is smaller than the experimental one, and the thickness measurements of the localized shear

Table 3
The measured thickness and shear strain and the calculated maximum temperature of the localized shear regions in hat-shaped specimens

Displacement (mm)		Initial temperature and material			
	77 K; as-received	190 K; as-received	298 K; as-received	298 K; shocked	
0.3	Shear strain	3.0	–	1.5	–
	Thickness (μm)	80	–	–	–
	T_{max} (K)	684	–	–	–
0.5	Shear strain	4.5	3.8	2.5	3.8
	Thickness (μm)	110	130	200	130
	T_{max} (K)	897	829	670	1100
1.0	Shear strain	–	5.3	5.0	6.7
	Thickness (μm)	–	190	200	150
	T_{max} (K)	–	1000	960	1650
1.4	Shear strain	–	–	5.5	7.7
	Thickness (μm)	–	–	200	180
	T_{max} (K)	–	–	1011	1800

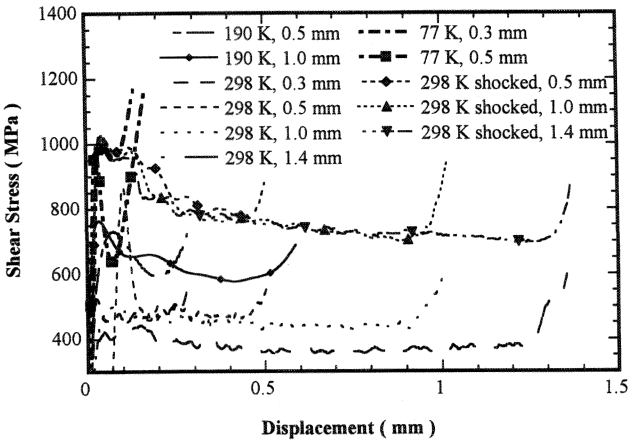

Fig. 13. Shear stress vs. displacement of hat-shaped specimens at different temperatures.

regions are all located above the prediction of Eq. (4). This difference may be due to the initiation mechanism and non-uniformity of the localized shear in such a particular geometrical configuration of hat-shaped specimens. In hat-shaped specimens, localized shear is initiated by the stress concentration at both ends of a localized shear region, while in other cases a shear band is initiated by the thermo-mechanical fluctuation at the site. The non-uniformity in the thickness of the localized shear regions in hat-shaped specimens is the evidence for this difference. As seen in Fig. 1, the thickness varies along the length of the localized shear region. Consequently, the strain and therefore the adiabatic temperature vary along the length of this region. The adiabatic temperature probably is higher at both ends of this region than at the middle which is listed in Table 3. If this non-uniformity were considered, the measured line should have been flatter. In this sense, the shear localization in hat-shaped specimens is really a 3-D

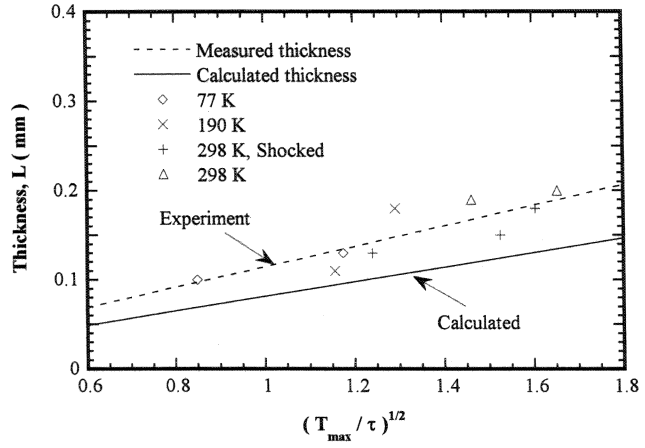

Fig. 14. Thickness of the localized shear regions in tantalum hat-shaped specimens as a function of the maximum temperature inside the region and shear stress acting on the region. Also plotted is the theoretical prediction using the model by Bai et al. [40,41].

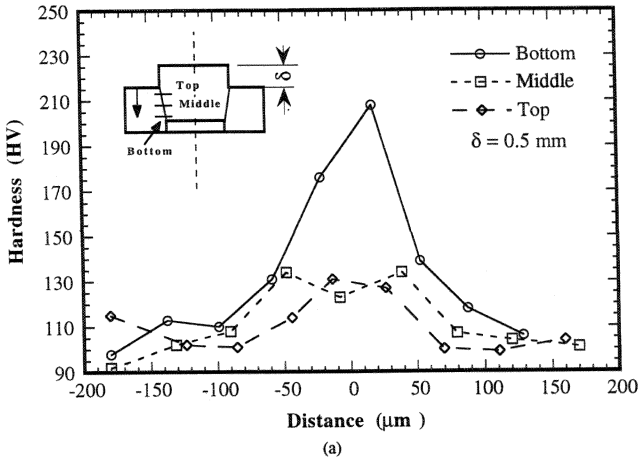

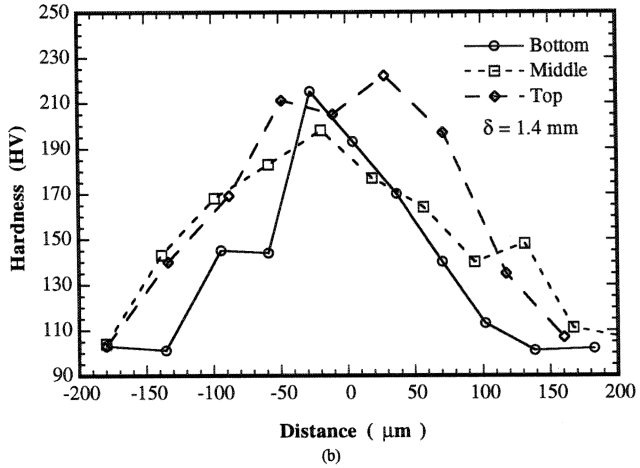

Fig. 15. Microindentation hardness as a function of distance across the localized shear regions at 298 K; prescribed displacement: (a) 0.5 mm and (b) 1.4 mm.

problem. Moreover, the thickness of the localized shear regions in hat-shaped specimens is also affected by the stress profile at their initiation stage. The stress profile is determined by the difference of diameters of the top plug and the underneath hole (Fig. 1a). The sharper stress profile may create a narrower region, although this effect may be reduced to a minimum when shear localization is fully developed. Therefore, the conditions experienced by the localized shear region of hat-shaped specimens are different from those under which Eq. (4) was derived.

This inhomogeneity of shear strain along the length of the localized shear region manifests itself in the differences of the residual microhardness along the length of localized shear regions, which are plotted in Fig. 15 for different displacements at 298 K and in Fig. 16 for different temperatures with the same displacement. Hardness profiles are shown for three positions along the localized shear region; they are indicated as top, middle, and bottom, respectively. For a displacement $\delta = 0.5$ mm ($\gamma = 2.5$) at 298 K, the hardness along the bottom traverse increases significantly more than

along the other traverses (Fig. 15a). At the higher displacements, such as $\delta = 1.4$ mm ($\gamma = 5.5$) at the same temperature as shown in Fig. 15(b), the differences of hardness in the corresponding sites have vanished. Lowering the temperature also causes such differences in hardness to vanish. Fig. 16 shows the hardness profiles of the specimens with a displacement of 0.5 mm at 190 and 77 K. Compared with Fig. 15(a), the differences of hardness in the different sites along the length of the localized shear region were reduced at 190 K (Fig. 16a) and further reduced at 77 K (Fig. 16b). The reduction of such differences in hardness profiles is another indicative of localized shear regions toward its fully-developed stage.

These differences of hardness along the band length are due to stress/strain concentrations at the sharp corners and variations in the band thickness, that can be seen in Fig. 11. These results indicate that variations in shear strain occur along the length of the localized shear region. Therefore, the shear strains measured at the middle of the bands as given in Table 3 are only minimum values in these bands and so are the estimations of the adiabatic temperature inside the localized shear regions. This can be responsible for the marked differences in TEM observations of deformed structures [5].

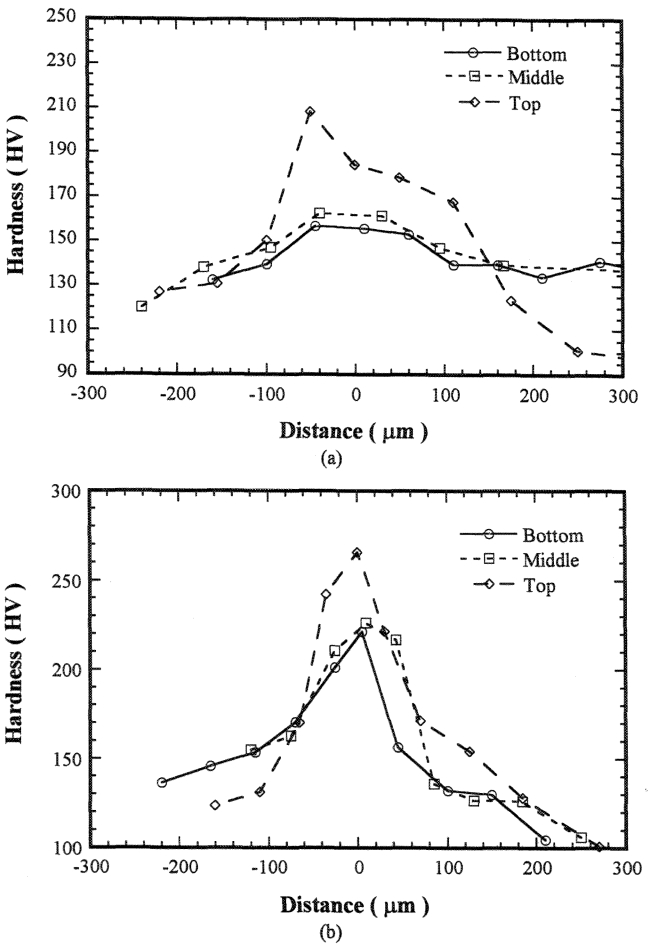

Fig. 16. Microindentation hardness as a function of distance across the localized shear regions; the prescribed displacement of 0.5 mm at: (a) 190 K and (b) 77 K.

3.3. Thick-walled cylinder tests

Unlike the formation of the localized shear region in hat-shaped specimens, which is due to the particular external tractions, shear bands formed in thick-walled cylinder samples are initiated through naturally occurring instabilities. A typical shear band pattern was reported in pure titanium by Nesterenko et al. [43]. The shear bands were spiral, starting at 45° about the radial direction at the initiation, which is the direction of maximum shear stress in this loading configuration.

Two collapsed tantalum specimens are shown in Fig. 17; (a) as-received material, (b) pre-shocked material. The central orifice was not completely collapsed. The residual radius is approximately 0.5 mm in Fig. 17(a), and it is larger for shocked tantalum in Fig. 17(b). This orifice is due to either jetting along the cylinder axis or to insufficient energy for collapse; it is more likely due to insufficient energy for shocked tantalum because of its higher strength. Nevertheless, over 90% of the process of collapse was successfully achieved. Cracks were also observed in the central orifice region. These cracks propagate mainly in shear localized regions very near the central orifice. With increasing radius, the shear bands become diffuse in both specimens.

For as-received tantalum (Fig. 17(a)), there are typically no shear bands. However, shear localization regions exist which are due to grain orientation softening and thermal fluctuation as analyzed by Nesterenko et al. [12] and Chen et al. [14]. The grains in the preferred orientation deform more and become softer than other adjacent grains. With the progress of deformation, this positive feed-back of thermal fluctuation causes more deformation in the grains originally in the preferred orientation and forms shear localization in these regions.

For shocked tantalum, the shear bands are clearly seen in Fig. 17(b). They are indicated by arrows. The trajectories of these shear bands are logarithm spirals and are typical for this geometry, as predicted by Nesterenko et al. [43]. Perhaps due to the incomplete collapse, the majority of shear bands are not well-developed. Fig. 17 shows better developed shear bands in the shocked tantalum than the as-received one. This is consistent with the results in cylindrical and hat-shaped specimens: shocked tantalum has a greater propensity to shear localization due to its higher strength imparted by plastic deformation during the shock compression process.

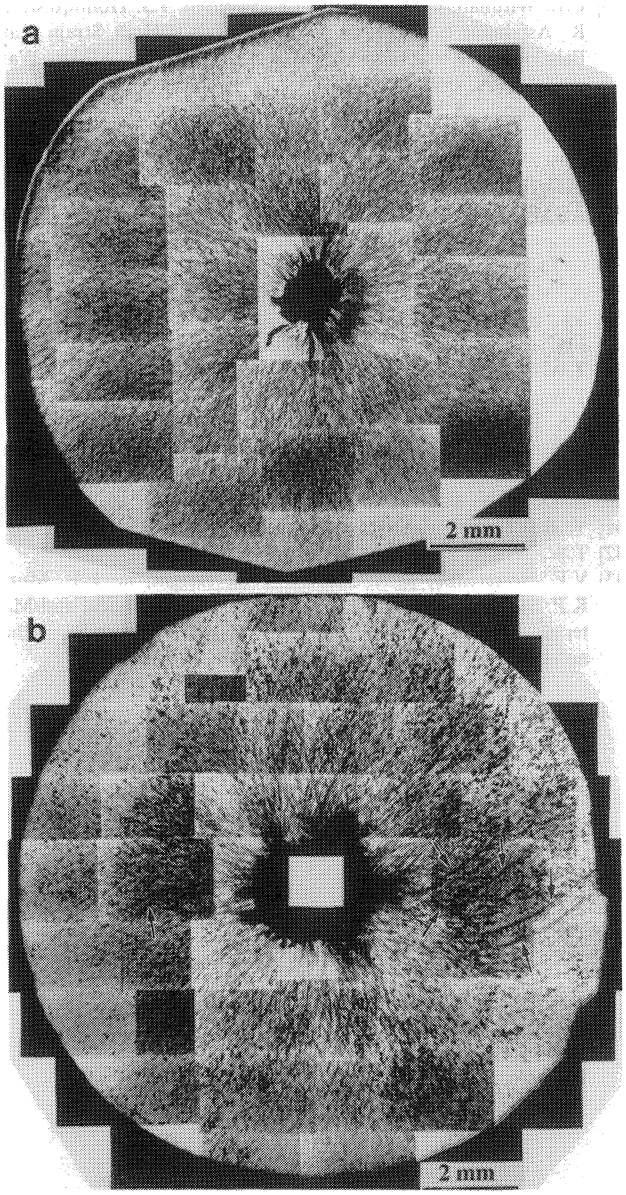

Fig. 17. Final configurations of thick-walled cylinder samples for (a) as-received tantalum, (b) shocked tantalum; notice shear bands, marked by arrows.

4. Conclusions

Shear localization was observed in tantalum deformed at low temperatures and high strain rates. The critical strain for shear localization increases with increasing temperature and decreases with increasing strain rate. The thickness of the forced localized shear regions was observed to decrease with decreasing temperature and to be reasonably well described by a simple equation proposed by Bai et al. [40,41]. The growth of localized shear regions in tantalum as studied with hat-shaped specimens exhibits a linear relationship with the square root of the ratio of the adiabatic temperature and the applied shear stress. Pre-shock conditioning increases the propensity of shear localization, as seen in all three techniques: cylindrical specimens, hat-shaped and thick-walled cylinder techniques.

Acknowledgements

This research was supported by the US Army Research Office through the URI (Contract No. DAAL03-92-G0108) and MURI (Contract No. DAAH04-96-1-0376) programs. The help of Dr M.P. Bondar and Y.L. Lukyanov of Lavrentiev Institute of Hydrodynamics, Novosibirsk, Russia, is greatly appreciated. J. Isaacs, UCSD, kindly performed the interrupted experiments reported in Fig. 6(a).

References

[1] E. Chen, A. Crowson, E. Lavernia, W. Ebihara, P. Kumar III (Eds.), Tantalum, TMS-AIME, Warrendale, PA, 1996.
[2] D. Lassila, G.T. Gray III, J. de Physique IV (Colloque) 1 (1991) 19–26.
[3] M.J. Worswick, N. Qiang, P. Niessen, R.J. Pick, in: M.A. Meyers, L.E. Murr, K.P. Staudhammer (Eds.), Shock-Wave and High-Strain-Rate Phenomena in Materials, Marcel Dekker, New York, 1992, pp. 87–95.
[4] N. Qiang, P. Niessen, R.J. Pick, Mater. Sci. Eng. A160 (1993) 49–53.
[5] M.A. Meyers, Y.-J. Chen, F.D.S. Marquis, D.S. Kim, Metall. Mater. Trans. A 26A (1995) 2493–2501.
[6] G.T. Gray III, K.S. Vecchio, Metall. Mater. Trans. 26A (1995) 2555–2563.
[7] A.J. Strutt, K.S. Vecchio, S.R. Bingert, G.T. Gray III, in: Proceedings of 1995 International Conference on W and Refractory Metals, MPIF, McLean, VA, 1995.
[8] S.R. Chen, G.T. Gray III, Metall. Mater. Trans. A 27A (1996) 2994–3006.
[9] L.E. Murr, M.A. Meyers, C.-S. Niou, Y.-J. Chen, S. Pappu, C. Kennedy, Acta Mater. 45 (1997) 157–175.
[10] T. Dummer, J.C. LaSalvia, G. Ravichandran, M.A. Meyers, Acta Mater. 17 (1998) 6267–6290.
[11] M.A. Meyers, V.F. Nesterenko, Y.J. Chen, J.C. LaSalvia, M.P. Bondar, Y.L. Lukyanov, in: L.E. Murr, K.P. Staudhammer, M.A. Meyers (Eds.), Metallurgical and Materials Applications of Shock-Wave and High-Strain-Rate Phenomena, Elsevier, Amsterdam, 1995, pp. 487–494.
[12] V.F. Nesterenko, M.A. Meyers, J.C. LaSalvia, M.P. Bondar, Y.J. Chen, Y.L. Lukyanov, Mater. Sci. Eng. A 229 (1997) 23–41.
[13] J.C. LaSalvia, Y.J. Chen, M.A. Meyers, V.F. Nesterenko, M.P. Bondar, Y.L. Lukyanov, in: E. Chen, A. Crowson, E. Lavernia, W. Ebihara, P. Kumar (Eds.), Tantalum, TMS-AIMS, Warrendale, PA, 1996, pp. 139–144.
[14] Y.J. Chen, J.C. LaSalvia, V.F. Nesterenko, M.A. Meyers, M.P. Bondar, Y.L. Lukyanov, Journal de Physique IV (Colloque) C3 (7) (1997) C3-435–C3-440.
[15] U.R. Andrade, M.A. Meyers, K.S. Vecchio, A.H. Chokshi, Acta Metall. Mater. 42 (1994) 3183–3195.
[16] M.A. Meyers, U.R. Andrade, A.H. Chokshi, Metall. Mater. Trans. 26A (1995) 2881–2893.
[17] L.W. Meyer, S. Manwaring, in: L.E. Murr, K.P. Staudhammer, M.A. Meyers (Eds.), Metallurgical Applications of Shock-Wave

and High-Strain-Rate Phenomena, Marcel Dekker, New York, 1986, p. 657.
[18] M.A. Meyers, G. Subhash, B.K. Kad, L. Prasad, Mech. Mater. 17 (1994) 175–193.
[19] R.W. Chen, K.S. Vecchio, Journal de Physique IV (Colloque) 4 (1994) C8/459–C8/464.
[20] V.F. Nesterenko, M.P. Bondar, I.V. Ershov, in: S.C. Schmidt, J.W. Shaner, G.A. Samara, M. Ross Jr. (Eds.), High-Pressure Science and Technology—1993, AIP Press, New York, 1994, p. 1173.
[21] R.F. Recht, J. Appl. Mech. 31 (1964) 189–193.
[22] Y. Bai, B. Dodd, Adiabatic Shear Localization: Occurrence, Theories and Applications, Pergamon, Oxford, 1992.
[23] R.J. Clifton, Material Response to Ultra High Loading Rates, Report No. NMAB-356, National Materials Advisory Board, NAS, Washington, DC, Ch. 8, 1979.
[24] G.Y. Chin, W.F. Hosford Jr., W.A. Backofen, Trans. Metall. Soc. AIME 230 (1964) 437–449.
[25] F.J. Zerilli, R.W. Armstrong, J. Appl. Phys. 68 (1990) 1580–1591.
[26] J.H. Bechtold, Acta Metall. 3 (1955) 249–254.
[27] K.G. Hoge, A.K. Mukherjee, J. Mater. Sci. 12 (1977) 1666–1672.
[28] T.E. Mitchell, W.A. Spitzig, Acta Metall. 13 (1965) 1169–1179.
[29] C.L. Wittman, C.M. Lopatin, J.P. Swensen, T.J. Holmquist, in: R. Asfahani, E. Chen, A. Crowson (Eds.), High Strain Rate Behavior of Refractory Metals and Alloys, TMS-AIME, Warrendale, PA, 1992, pp. 167–178.
[30] F.J. Zerilli, R.W. Armstrong, J. Phys. IV (France) 7 (1997) C3-637–C3-642.
[31] T.W. Wright, J.W. Walter, J. Mech. Phys. Solids 35 (1987) 701–720.
[32] A. Molinari, R.J. Clifton, C.R. Acad. Sci. Paris, 296 (1983) Series II, 1–4.
[33] C. Fressengeas, A. Molinari, J. Mech. Solids 35 (1987) 185–211.
[34] A. Molinari, R.J. Clifton, J. Appl. Mech. 54 (1987) 806–812.
[35] S.L. Semiatin, M.R. Staker, J.J. Jonas, Acta Metall. 32 (1984) 1347–1354.
[36] T.W. Wright, J. Mech. Phys. Solids 38 (1990) 515–530.
[37] T.W. Wright, Mech. Mater. 17 (1994) 215–222.
[38] Z.S. Basinski, Proc. R. Soc. (Lond.) A240 (1957) 229–242.
[39] S. Takeuchi, E. Kuramoto, T. Suzuki, Acta Metall. 20 (1972) 909–915.
[40] B. Dodd, Y. Bai, Mater. Sci. Tech. 1 (1985) 38–40.
[41] Y. Bai, C. Cheng, S. Yu, Acta Mech. Sinica 2 (1986) 1–7.
[42] T.W. Wright, J. Mech. Phys. Solids 35 (1987) 269–282.
[43] V.F. Nesterenko, M.A. Meyers, T.W. Wright, in: L.E. Murr, K.P. Staudhammer, M.A. Meyers (Eds.), Metallurgical and Materials Applications of Shock Wave and High-Strain-Rate Phenomena, Elsevier, Amsterdam, 1996, pp. 397–404.

Instructions for Authors

SUBMISSION OF PAPERS

Manuscripts for the main part of the journal and for the Letters Section should be submitted as follows:

For authors in Europe

Professor Gernot Kostorz
ETH Zurich
Institut für Angewandte Physik
CH-8093 Zurich, Switzerland
Fax: +41 (1633) 1105

For authors in Japan

Professor Masahiro Koiwa
Department of Materials Science and Engineering
Faculty of Engineering
Kyoto University
Yoshida-Honmachi, Sakyo-ku
Kyoto 606-8501, Japan
Fax: +81 (75) 753 4861

For authors in North and South America and the rest of the world

Professor Carl C. Koch
North Carolina State University
Department of Materials Science and Engineering
233 Riddick Building
Stinson Drive
Raleigh, NC 27695-7907, USA
Fax: +1 (919) 515 7724
or
Professor Enrique J. Lavernia
Department of Chemical & Biochemical Engineering & Materials Science
University of California Irvine
Irvine, CA 92697-2540, USA
Tel/Fax: +1 949 824 4040

Manuscripts

Three copies should be submitted to the Editor, in double-spaced typing on pages of A4 size and with wide margins (Letters should not exceed 2000 words and a maximum of 5 figures). All tables and illustrations should bear a title or legend.
An *abstract* should accompany reviews, original papers and Letters. It should present (preferably in 100–150 words; 50 words or less for Letters) a brief and factual account of the contents and conclusions of the paper, and an indication of the relevance of new material.

References should be indicated by numerals in square brackets, introduced consecutively and appropriately in the text.

References must be listed on separate sheet(s) at the end of the paper. Every reference appearing in the text should be quoted in the reference list, and *vice versa*. When reference is made to a publication written by more than two authors it is preferable to give only the first author's name in the text followed by "*et al.*". However, in the list of references the names and initials of all authors must be given.

Three sets of figures should be submitted. One set of line drawings should be in a form suitable for reproduction, drawn in Indian ink on drawing or tracing paper (letter height, 3–5 mm). Alternatively, such illustrations may be supplied as high contrast, black-and-white glossy prints. Duplicate original micrographs should be provided wherever possible to facilitate the refereeing process. Magnifications should be indicated by a ruled scale bar on the micrograph. Captions to illustrations should be typed in sequence on a separate page.

All abbreviated terms must be defined when first used (both in the abstract and in the text) and authors must express all quantities in SI units, with other units in parentheses if desired.
Authors in Japan please note that information about how to have the English of your paper checked, corrected and improved (before submission) is available from: Elsevier Science K.K. Japan, Higashi-Azabu 1-chome Building 4F, 1-9-15 Higashi-Azabu, Minato-ku, Tokyo 106-0044, Japan. Tel: +81-3-5561-5032; Fax: +81-3-5561-5045.

Further information

All questions arising after the acceptance of manuscripts, especially those relating to proofs, should be directed to: Elsevier Science Ireland, Elsevier House, Brookvale Plaza, East Park, Shannon, Co. Clare, Ireland. Tel.: +353 61 709640; fax: +353 61 709107.

Submission of electronic text

The final text may be submitted on a 3.5 in or 5.25 in diskette (in addition to a hard copy with original figures). Double density (DD) or high density (HD) diskettes are acceptable, but must be formatted to their capacity before the files are copied on to them. The main text, list of references, tables and figure legends should be stored in separate text files with clearly identifiable file names. The format of these files depends on the word processor used. WordPerfect 5.1 is the most preferable but for other formats please refer to the Instructions to Authors booklet. It is *essential* that the name and version of the wordprocessing program, type of computer on which the text was prepared, and format of the text files are clearly indicated.
The final manuscript may contain last minute corrections which are not included in the electronic text but such corrections must be clearly marked on the hard copy.